THE JOURNAL OF BIOLOGICAL CHEMISTRY
Vol. 276, No. 6, Issue of February 9, pp. 3999–4011, 2001

Printed in U.S.A.

Molecular and Functional Characterization of a Family of Rat Brain T-type Calcium Channels*

Received for publication, September 7, 2000, and in revised form, November 8, 2000
Published, JBC Papers in Press, November 9, 2000, DOI 10.1074/jbc.M008215200

John E. McRory‡§, Celia M. Santi‡§, Kevin S. C. Hamming‡, Janette Mezeyova¶, Kathy G. Sutton‡, David L. Baillie‖, Anthony Stea, and Terrance P. Snutch‡ ‡‡**

*From the ‡Biotechnology Laboratory, University of British Columbia, Vancouver, British Columbia V6T 1Z3, Canada, ¶NeuroMed Technologies Inc., Vancouver, British Columbia V6T 1Z4, Canada, the ‖Department of Molecular Biology and Biochemistry, Simon Fraser University, Burnaby, British Columbia V5A 1S6, Canada, and **University-College of the Fraser Valley, Abbotsford, British Columbia V2S 7M8, Canada*

Voltage-gated calcium channels represent a heterogenous family of calcium-selective channels that can be distinguished by their molecular, electrophysiological, and pharmacological characteristics. We report here the molecular cloning and functional expression of three members of the low voltage-activated calcium channel family from rat brain (α_{1G}, α_{1H}, and α_{1I}). Northern blot and reverse transcriptase-polymerase chain reaction analyses show α_{1G}, α_{1H}, and α_{1I} to be expressed throughout the newborn and juvenile rat brain. In contrast, while α_{1G} and α_{1H} mRNA are expressed in all regions in adult rat brain, α_{1I} mRNA expression is restricted to the striatum. Expression of α_{1G}, α_{1H}, and α_{1I} subunits in HEK293 cells resulted in calcium currents with typical T-type channel characteristics: low voltage activation, negative steady-state inactivation, strongly voltage-dependent activation and inactivation, and slow deactivation. In addition, the direct electrophysiological comparison of α_{1G}, α_{1H}, and α_{1I} under identical recording conditions also identified unique characteristics including activation and inactivation kinetics and permeability to divalent cations. Simulation of α_{1G}, α_{1H}, and α_{1I} T-type channels in a thalamic neuron model cell produced unique firing patterns (burst *versus* tonic) typical of different brain nuclei and suggests that the three channel types make distinct contributions to neuronal physiology.

Voltage-sensitive calcium channels mediate the rapid, voltage-dependent entry of calcium into many types of nerve, muscle, and endocrine cells. In the nervous system, calcium entry contributes toward the electrical properties of neurons, modulates calcium-dependent enzymes and ion channels, controls calcium-dependent gene transcription, and initiates the release of neurotransmitters and neuromodulators. Electrophysiological analyses have categorized native calcium currents into two major classes that differ in their voltage activation properties. High voltage-activated (HVA)[1] calcium channels represent a diverse family of channels that first activate at relatively depolarized potentials (usually > -40 mV) and that display distinct pharmacological characteristics (L-type, N-type, P/Q-type, and R-type; Refs. 1 and 2). In contrast to activation for HVA calcium channels, low voltage-activated (LVA or T-type) calcium channels first activate with relatively small depolarizations (between -80 and -60 mV) and have a poorly defined pharmacology. In addition to their distinct low voltage dependence of activation, T-type calcium channels also exhibit unique voltage-dependent kinetics, small single channel conductance, rapid inactivation, slow deactivation, and a relatively higher permeability to Ca^{2+} compared with Ba^{2+} (3).

The initial evidence for the existence of LVA calcium currents was obtained from neurons of the inferior olivary nucleus by Llinas and Yarom (4). Subsequently, LVA currents were recorded from cells isolated directly from the dorsal root ganglia (5–9), pituitary (10, 11), and cardiac myocytes (12–16). T-type channels are of interest, since they are responsible for rebound burst firing in central neurons and are implicated in normal brain functions such as slow wave sleep and in diseased states such as epilepsy (3, 17). They are also thought to play a role in hormone secretion (18, 19) and smooth muscle excitability (20). The biophysical characterization of T-type channels has been complicated by the presence of multiple types of calcium currents in neurons and other cells as well as a lack of specific pharmacological tools. In addition, there is considerable heterogeneity in the reported activation, inactivation, permeation, and pharmacology of neuronal T-type currents. T-type calcium channels represent the most recent calcium channel family to be described at the molecular level (21–25), although there remains little known concerning their biochemical composition.

In the present paper, the molecular and electrophysiological characteristics of three members of the rat brain T-type calcium channel family (α_{1G}, α_{1H}, and α_{1I}) are reported. This is the first report defining the molecular and biophysical properties of three distinct T-type calcium channels isolated from the same tissue and species. Electrophysiological recordings describe α_{1G}, α_{1H}, and α_{1I} currents with many distinguishing characteristics typical of T-type currents present in native cells, although they each also possess distinct kinetics, inactivation

* This work was supported by a grant from the Canadian Institutes for Health Research (CIHR) (to T. P. S.); fellowship support from the Human Frontiers Research Program (to C. M. S), from the CIHR (to J. E. M.), and from the Natural Sciences and Engineering Research Council of Canada and Killam Foundation (to K. S. C. H.); and a CIHR Senior Scientist Award (to T. P. S.). The costs of publication of this article were defrayed in part by the payment of page charges. This article must therefore be hereby marked "*advertisement*" in accordance with 18 U.S.C. Section 1734 solely to indicate this fact.

The nucleotide sequence(s) reported in this paper has been submitted to the GenBank™/EBI Data Bank with accession number(s) AF290212 (α_{1G}), AF290213 (α_{1H}), and AF290214 (α_{1I}).

§ These authors contributed equally to this work.

‡‡ To whom correspondence should be addressed: Biotechnology Laboratory, Rm. 237-6174 University Blvd., University of British Columbia, Vancouver, British Columbia V6T 1Z3, Canada. Tel.: 604-822-6968; Fax: 604-822-6470; E-mail: snutch@zoology.ubc.ca.

[1] The abbreviations used are: HVA, high voltage-activated; aa, amino acid(s); bp, base pair; kb, kilobase(s); HEK, human embryonic kidney; LVA, low voltage-activated; PCR, polymerase chain reaction; RT, reverse transcription; TEA, tetraethylammonium; CNS, central nervous system.

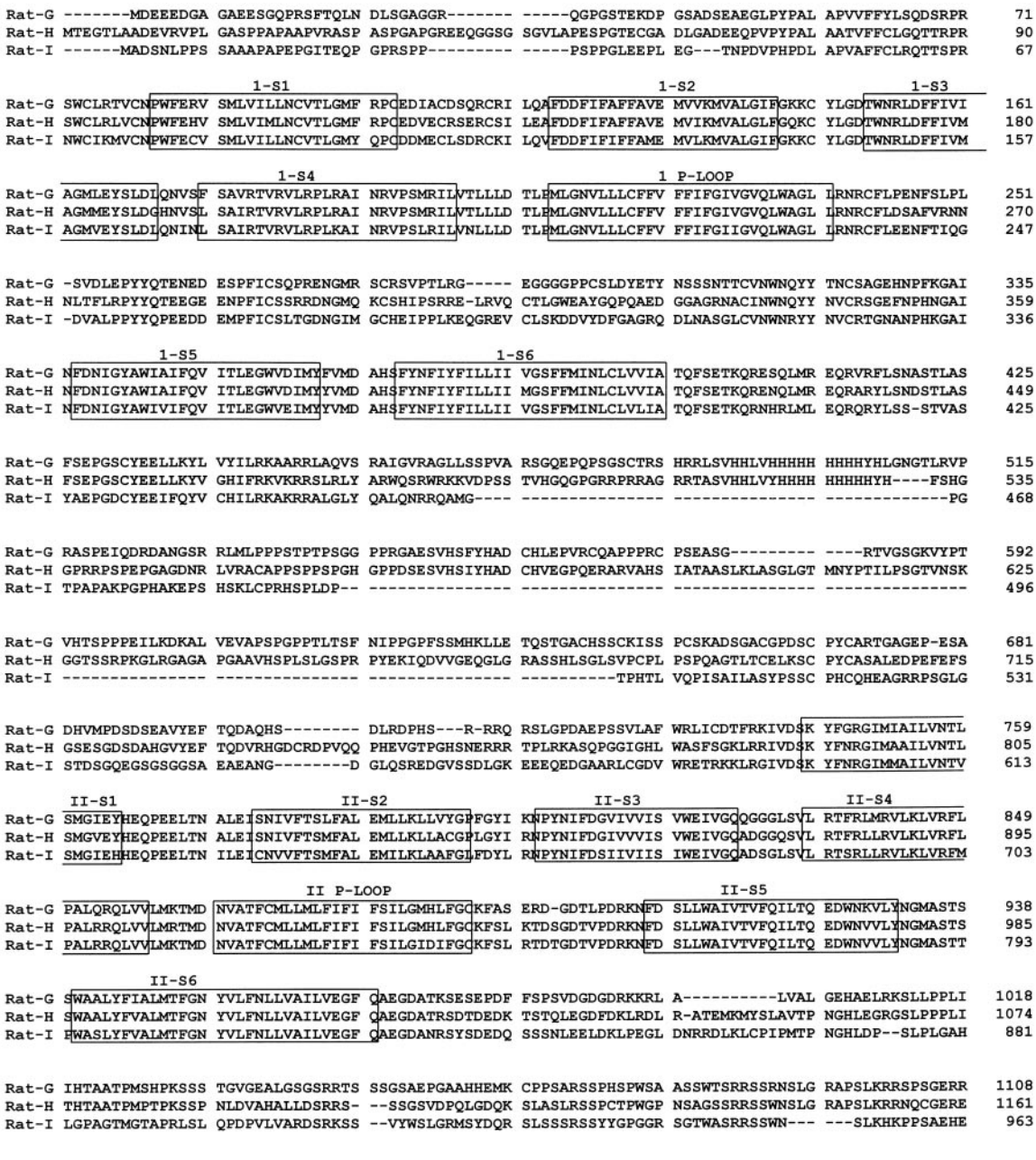

FIG. 1. **Primary structure of the rat brain α_{1G}, α_{1H}, and α_{1I} T-type calcium channels.** Transmembrane regions (S1–S6) and pore regions (P-loop) are *boxed*, while *dashes* represent gaps introduced to align the three full-length cDNA sequences.

profiles, and divalent ion permeabilities. We also find evidence for the generation of multiple α_{1I} variants by alternative splicing and for the unique developmental and spatial expression of α_{1G}, α_{1H}, and α_{1I} T-type calcium channels in the rat CNS.

MATERIALS AND METHODS

Molecular Cloning of Rat Brain T-type Channels—To identify novel calcium channel subtypes, oligonucleotides were designed based on structurally conserved elements found in all cloned mammalian HVA calcium channels (rat brain α_{1A}, GTCAAAACTCAGGCCTTCTA and AACGTGTTCTTGGCTATCGCGGTG; rat brain α_{1B}, GTGAAAGCACAGAGCTTCTACTGG and AACGTTTTCTTGGCCATTGCTGTG; rat brain α_{1C}, GTTAAATCCAACGTCTTCTACTGG and AATGTGTTCTTGGCCATTGCGGTG; rat brain α_{1D}, GTGAAGTCTGTCACGTTTTACTGG and AAGCTCTTCTTGGCCATTGCTGTA; rat brain α_{1E}, GTCAAGTCGGCAAGTGTTCTTA and AATGTATTCTTGGCTATCGC). The oligonucleotide sequences were subsequently utilized to "screen" the

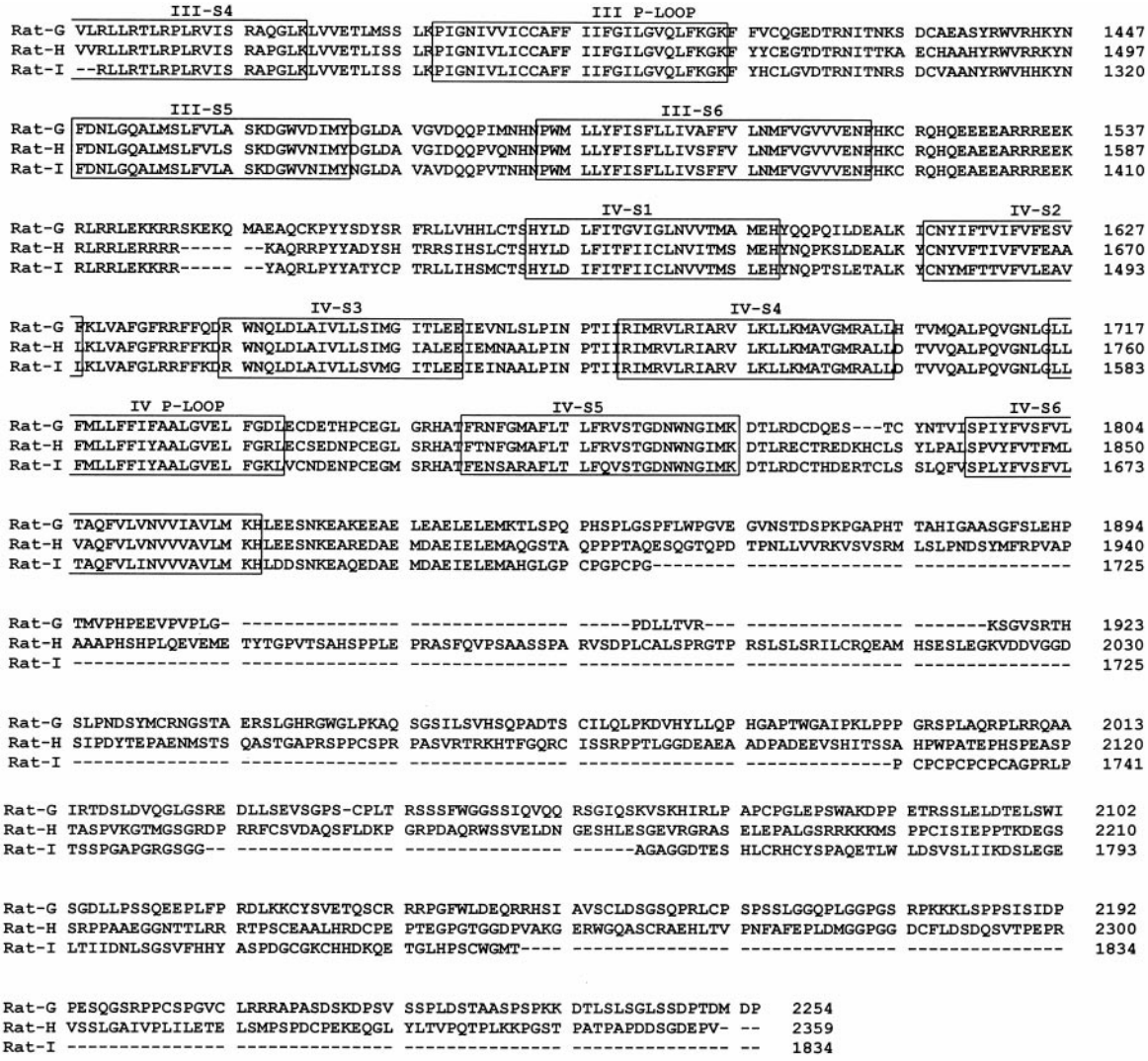

FIG. 1—*continued*

entire *Caenorhabditis elegans* genome data base (ACeDB) and resulted in the identification of five potential voltage-dependent ion channels in *C. elegans* (cosmids and reading frames: C11D2.6, C27F2.3, C54D2.5, C48A7.1, and T02C5.5). Three of the *C. elegans* genes (C54D2.5, C48A7.1, and T02C5.5) were determined to represent homologues of rat and human calcium channels expressed in nerve, muscle, and cardiovascular tissues, while the other two genes (C11D2.6 and C27F2.3) represent novel four domain-type ion channels. The T02C5.5 open reading frame encodes the *unc-2* gene, which is a calcium channel α_1 subunit homologous to the mammalian α_{1A}, α_{1B}, and α_{1E} subtypes, while C48A7.1 encodes *egl-19*, a nematode calcium channel α_1 subunit homologous to the mammalian α_{1C}, α_{1D}, α_{1F}, and α_{1S} L-type channels. Mammalian homologues of the *C. elegans* C54D2.5 reading frame were identified by "screening" the GenBank™ expressed sequence tag data bank with C54D2.5. Four of the resulting human expressed sequence tags (H55225, H55617, H55223, and H55544) were judged to encode novel calcium channel-like proteins. Utilizing these sequences, synthetic oligonucleotide primers were generated and used to amplify human brain total RNA and identified a 567-bp fragment corresponding to a portion of human brain α_{1I}.

The 567-bp human polymerase chain reaction (PCR) fragment was labeled by random priming and used to screen 750,000 plaque-forming units of a rat brain cDNA library enriched for cDNAs greater than 4 kb (26). After four rounds of screening, 28 positives were isolated, and their ends were sequenced. Of these, 19 encoded for α_{1G}, four for α_{1H}, and five for the α_{1I} subunit. The full-length rat brain α_{1G}, α_{1H}, and α_{1I} clones were assembled in pBluescript SK from overlapping cDNAs. Both strands of the full-length clones were sequenced using a modified dideoxynucleotide protocol and Sequenase version 2.1 (U.S. Biochemical Corp.) and then subcloned into the vertebrate expression vector pCDNA-3 (Invitrogen).

Isolation of α_{1I} Splice Variants—Isoforms of the α_{1I} subunit were identified by DNA sequence analysis of multiple rat brain α_{1I} cDNA clones. To confirm that the clones represented *bona fide* expressed transcripts, reverse transcriptase and PCR (RT-PCR) was performed with total rat brain RNA. The reactions consisted of 1 μg of RNA, 1× RT buffer, 10 mM dNTPs, 5 units of RT (Life Technologies, Inc.), and 10 pmol of the 3′-oligonucleotide at 42 °C for 90 min. The 50-μl PCR was composed of 1 μl of rat brain cDNA/RNA, 1× PCR buffer, 1.25 mM dNTPs, 2 units of *Taq* polymerase, and 20 pmol of each oligonucleotide (variant 1, 5′-ACTCTGGAAGGCTGGGTGGAG-3′ and 5′-GAGAACGAGGCACAAGTTGATC-3′; variant 2, 5′-ATGGGTACTGCCCCCCGCCTCTCA-3′ and 5′-CAAGGATCGCTGATCATAGCTC-3′; and variant 3, 5′-ATCCGTATCATGCGTGTTCTGCG-3′ and 5-CCACTGGCAGAGCTGTACACTG-3′). The reactions were preheated for 15 min at 95 °C followed by 35 cycles of 30 s at 95 °C, 20 s at 55 °C, and 1 min at 72 °C. The fidelity of all three variants and the wild type α_{1I} cDNA was confirmed by sequencing of both strands.

Deduction of Intron-Exon Boundaries—To confirm that the α_{1I} isoforms represented alternatively spliced variants of the α_{1I} gene, PCR was used to amplify portions of rat genomic DNA flanking the regions of interest. Oligonucleotides on either side of the putative introns were synthesized for use in the PCR to determine splice variants (as above). The 50-μl PCR was composed of 1 ng of rat genomic DNA, 1× PCR buffer, 1.25 mM dNTPs, 2 units of *Taq* polymerase, and 20 pmol of each oligonucleotide. The reactions were placed into a preheated PCR block for 15 min at 95 °C followed by 35 cycles (30 s at 95 °C, 20 s at 55 °C, 1 min at 72 °C). The PCR products were separated by electrophoresis through a 1.5% agarose gel, blotted to a nylon membrane, and then probed with a γ-^{32}P-radiolabeled intron-specific oligonucleotide probe to

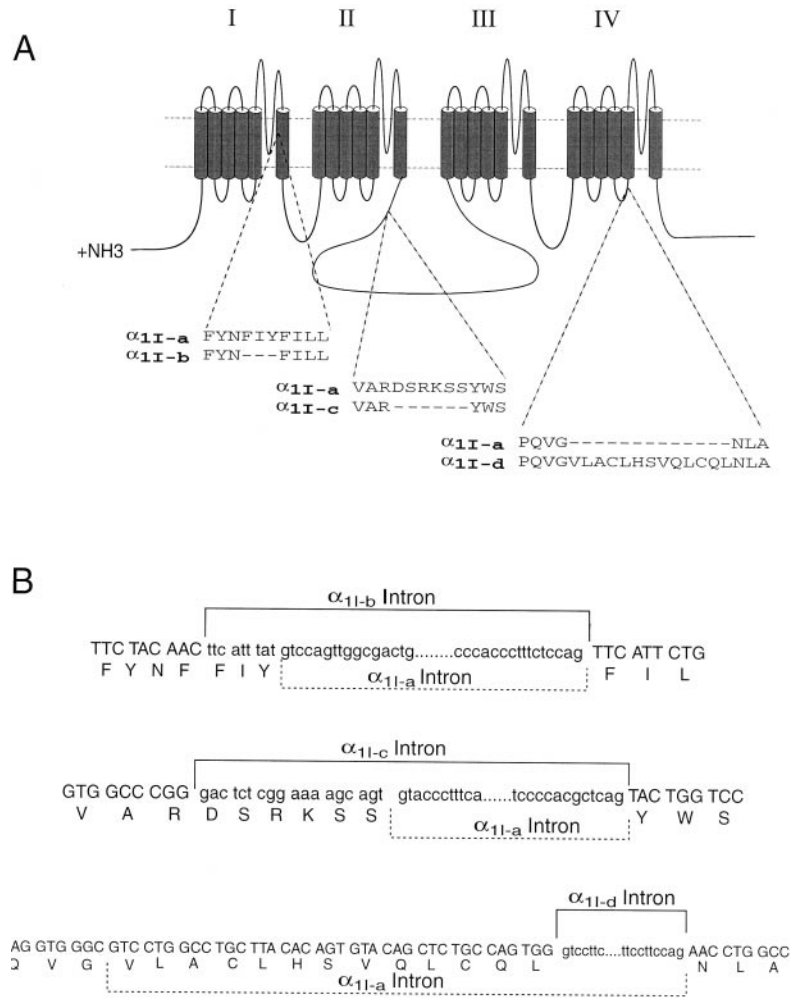

FIG. 2. **Alternatively spliced isoforms of the α_{1I} T-type channel.** *A*, schematic structure of the T-type α_1 subunit and primary structure comparing differences between wild type $\alpha_{1I\text{-}a}$ subunit and three other α_{1I} variants isolated by cDNA cloning from rat brain. *B*, comparison of cDNA and rat genomic DNA sequence of the $\alpha_{1I\text{-}a}$, $\alpha_{1I\text{-}b}$, $\alpha_{1I\text{-}c}$, and $\alpha_{1I\text{-}d}$ isoforms.

identify the genomic band of interest. Fragments hybridizing to the probes were cut out and cloned into pGem-T Easy (Promega), and their DNA sequence was determined.

RNA Isolation and Northern Blot—Total cellular RNA was isolated from adult rat tissues; Northern blot analysis was performed with RNA size markers (Life Technologies), total RNA (30 μg/lane) from spinal cord, pons/medulla, cerebellum, striatum, hypothalamus/thalamus, hippocampus, cortex, olfactory bulb, and whole brain; and separated through a 1.1% agarose gel containing 1.1 M formaldehyde and then transferred to Hybond-N nylon membrane by capillary blot. Hybridization was performed independently for each α_1 subunit, and the radiolabeled probe was allowed to decay between probe hybridization. Northern blot hybridization conditions utilized 5× SSPE, 0.3% SDS, 10 μg/μl tRNA, 30 μg/μl salmon sperm blocking DNA, and a random-primed cDNA probe that corresponds to nucleotides 2523–3397 of the α_{1I} clone, 3568–4426 of the α_{1G} clone, or 3391–4231 of the α_{1H} cDNA clone.

Reverse Transcription and Polymerase Chain Reaction—To detect low levels of T-type channel expression, RT-PCR analysis of T-type channel expression within different brain regions was performed. The reaction consisted of 1 μg of RNA, 1× RT buffer, 10 mM dNTPs, 5 units of RT (Life Technologies), and 10 pmol of the α_{1G} oligonucleotide (5′-CAGGAGACGAAACCTTGA-3′) α_{1H} oligonucleotide (5′-GGAGACGCGTAGCCTGTT-3′), or α_{1I} oligonucleotide (5′-CAGGATCCGGAACTTGTT-3′) at 42 °C for 90 min. From this reaction, 5 μl was removed and added to a 50-μl PCR composed of 1× PCR buffer, 1.25 mM dNTPs, 2 units of *Taq*, 20 pmol of the 3′-oligonucleotide, and 20 pmol of the 5′-oligonucleotide (α_{1G}-5′-TCAGAGCCTGATTTCTTT-3′, α_{1H}-5′-GACGAGGATAAGACGTCT-3′, or α_{1I}-5′-GATGAGGACCAGAGCTCA-3′). The reactions were placed into a preheated PCR block for 35 cycles (1 min at 95 °C, 45 s at 55 °C, 45 s at 72 °C). The PCR products were separated by electrophoresis through a 1.5% agarose gel, blotted to a nylon membrane, and then probed with a γ-^{32}P-radiolabeled oligonucleotide probe specific for each of the three channels. As a positive control, 1 μg of RNA from each brain region was amplified by 35 cycles (1 min at 95 °C, 30 s at 55 °C, 30 s at 72 °C) with α-tubulin oligonucleotides (5′-CAGGTGTCCACGGCTGTGGTG-3′ and 5′-AGGGCTCCATCGAAACGCAG-3′).

Transient Transfection and Electrophysiology—Human embryonic kidney cells (HEK293; tsa-201) were grown in standard Dulbecco's modified Eagle's medium, supplemented with 10% fetal bovine serum and 50 units/ml penicillin streptomycin to 80% confluence. Cells were maintained at 37 °C in a humidified atmosphere of 95% O_2 and 5% CO_2, and every 2–3 days they were enzymatically dissociated with trypsin-EDTA and plated on 35-mm Petri dishes 12 h prior to transfection. A standard calcium phosphate procedure was used to transiently transfect cells. Rat α_{1G} (3 μg), rat α_{1H} (3 μg), and rat α_{1I} (3 μg) calcium channel subunits were cotransfected with CD8 (2 μg) marker plasmid, and 15 μg pBluescript SK carrier DNA for a total of 20 μg of cDNA. Transiently transfected cells were selected for expression of CD8 by adherence of Dynabeads as described previously (27).

Functional expression in transfected cells was evaluated 24–48 h after transfection using the whole-cell patch clamp technique (28). The external recording solution contained (unless otherwise noted) 2 mM $CaCl_2$, 1 mM $MgCl_2$, 10 mM HEPES, 40 mM TEA-Cl, 92 mM CsCl, 10 mM glucose, pH 7.2. The internal pipette solution contained 105 mM CsCl, 25 mM TEA-Cl, 1 mM $CaCl_2$, 11 mM EGTA, 10 mM HEPES, pH 7.2. Whole-cell currents were recorded using an Axopatch 200B or 200A amplifier (Axon Instruments, Foster City CA), controlled and monitored with a PC running pCLAMP software version 6.03 (Axon Instruments). Patch pipettes (Sutter borosilicate glass BF150-86-10) were pulled using a Sutter P-87 puller and fire-polished using a Narishige microforge, and they showed a resistance of 2.5–4 megaohms when filled with internal solution. Series resistance had typical values of 7–10 megaohms and was electronically compensated by at least 60%. Whole-cell currents never exceeded 2 nA, limiting errors in voltage to a few mV. Only cells exhibiting adequate voltage control (judged by smoothly rising current-voltage (*I*-V) relationship and monoexponential decay of capacitive currents) were included in the analysis. The bath was connected to ground via a 3 M KCl agar bridge. Gigaohm seals were formed directly in the external control solution, and all recordings were performed at room temperature (20–24 °C). Data were low pass-filtered at

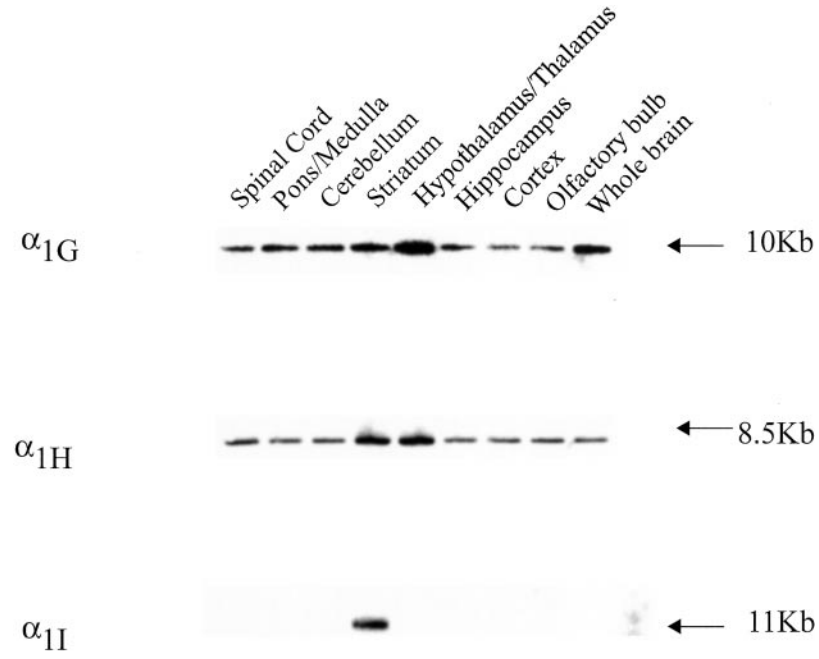

FIG. 3. **Northern blot analysis of T-type calcium channels in the rat central nervous system.** Autoradiograms are shown of Northern blot hybridization of α_{1G}, α_{1H}, and α_{1I} cDNA probes specific to the II-III linker region of each channel subtype. Each *lane* contains 30 μg of total RNA. The sizes of the α_{1G}, α_{1H}, and α_{1I} transcripts were determined using RNA standards (Life Technologies, Inc.). Autoradiograms were exposed to film for 3 days at −80 °C with intensifying screens.

2 kHz using the built-in Bessel filter of the amplifier, and in most cases, subtraction of capacitance and leakage current was carried out on-line using the P/4 protocol. Recordings were analyzed using Clampfit 6.03 (Axon Instruments), and figures and fittings utilized the software program Microcal Origin (version 3.78).

Data Analysis and Modeling—Calcium current activation curves were constructed by converting the peak current values from the *I*-V relationships to conductance using the equation $g\mathrm{Ca} = I_{peak}/(V_c - E_{Ca})$, where I_{peak} is the peak calcium current, V_c the command pulse potential, and E_{Ca} the apparent calcium reversal potential obtained by linear extrapolation of the current values in the ascending portion of the *I*-V curve. Conductance values were then normalized and fitted to standard Boltzman relations: $g/g_{max} = (1 + (\exp(-V - V_{0.5a})/k_a)) - 1$, where g is the peak conductance, g_{max} is the maximal peak calcium conductance, $V_{0.5a}$ is the midpoint of the activation curve, and k_a is the activation slope factor. Steady-state inactivation curves were obtained by evoking calcium currents with a test depolarization to −30 mV applied at the end of 15-s prepulses from −120 to −50 mV. The steady-state inactivation curves were constructed by plotting the normalized current during the test pulse as a function of the conditioning potential. The data were fitted with a Boltzman equation: $I/I_{max} = (1 + \exp((V - V_{0.5i}/k_i)) - 1$, where I is the peak current, I_{max} is the peak current when the conditioning pulse was −120 mV, V and $V_{0.5i}$ are the conditioning potential and the half-inactivation potential, respectively, and k_i is the inactivation slope factor.

The electrophysiological properties of the α_{1G}, α_{1H}, and α_{1I} channels were modeled using modified Hodgkin-Huxley equations for T-type calcium channels produced by Huguenard and McCormick (29). The values for voltage-dependent activation and inactivation, as well as the time constants for activation, inactivation, and deactivation were obtained from whole-cell recordings of α_{1G}, α_{1H}, or α_{1I} using 2 mM calcium as the charge carrier. These values were substituted for the data obtained from recordings of T-type calcium currents of juvenile rat thalamic relay neurons (29). Simulated current clamp recordings of thalamic relay neurons were generated using the C-Clamp software program based on the major currents of these cells (30) and substitution of α_{1G}, α_{1H}, or α_{1I} for the native T-type currents.

RESULTS

Screening of an expressed sequence tag data bank with the *C. elegans* C54D2.5 open reading frame described several unidentified human expressed sequence tag sequences (H55225, H55617, H55223, and H55544), which were then used to design synthetic oligonucleotides and amplify a 567-bp α_{1I} subunit fragment from human brain total RNA (see Ref. 21 for an alternative strategy). Utilizing the human 567-bp fragment as a probe, full-length rat brain cDNAs homologous to C54D2.5 were isolated from a rat brain cDNA library and shown by sequence analysis to encode three different members of the T-type calcium channel family (α_{1G}, α_{1H}, and α_{1I}) (Fig. 1). Similar to HVA calcium channels and sodium channels, all three putative rat brain T-type channel subunits possess four structural domains linked by intracellular loops, a conserved pore region (P-loop), and voltage sensors (S4 segments) in each of the four domains. In contrast to the HVA calcium channel subunits, which all possess a conserved glutamate within their P-loops, the T-type channels have aspartate residues substituted in domain III and IV P-loops. Additional differences from HVA channels include no apparent β-subunit binding site in the domain I-II linker (31) and no EF hand region (32) or calmodulin binding site (33, 34) in the carboxyl tail.

While the α_{1G} and α_{1H} subunits encode proteins of 2254 and 2359 amino acids (aa), respectively, the α_{1I} subunit encodes for a significantly shorter protein of 1826 aa, which is mostly due to a shorter domain I-II linker (199 aa for α_{1I} *versus* 345 and 368 aa for α_{1G} and α_{1H}, respectively) and a shorter carboxyl tail region (77 aa for α_{1I} *versus* 433 and 493 aa for α_{1G} and α_{1H}, respectively). The overall conservation of aa sequence is highest between the α_{1G} and α_{1H} subunits (56% identity), with the α_{1I} protein having 53% identity to α_{1H} and 49% identity to α_{IG}. Most of the sequence conservation is found in the membrane-spanning regions with substantially less identity in the carboxyl tail and putative intra- and extracellular loops.

Sequence analysis of additional α_{1I} cDNAs showed that at least four α_{1I} variants are expressed in rat brain. Compared with the "wild type" $\alpha_{1I\text{-}a}$ isoform, the predicted primary sequence of the $\alpha_{1I\text{-}b}$ variant is missing three residues (FIY) in domain I S6, the $\alpha_{1I\text{-}c}$ variant has a six-aa deletion in the domain II-III linker, and the $\alpha_{1I\text{-}d}$ variant contains a 13-aa insertion in the putative cytoplasmic linker between domain IV S4 and S5 (Fig. 2*A*). Since variations in cDNA sequence may be due to RT artifacts, it is important to confirm that putative variants are in fact encoded in the genome. Along this line, rat genomic DNA was examined in the regions flanking the putative splice junctions of the α_{1I} variants. Fig. 2*B* shows that the $\alpha_{1I\text{-}b}$, $\alpha_{1I\text{-}c}$, and $\alpha_{1I\text{-}d}$ variants all result from the apparent use of alternative 5′ splice junction sites. In the case of $\alpha_{1I\text{-}d}$, the alternative 5′ junction matches the 5′ GT splice consensus site, while in $\alpha_{1I\text{-}b}$ and $\alpha_{1I\text{-}c}$ the 5′ sites are nontypical TT and GA intronic junctions. RT-PCR of adult rat brain RNA confirmed

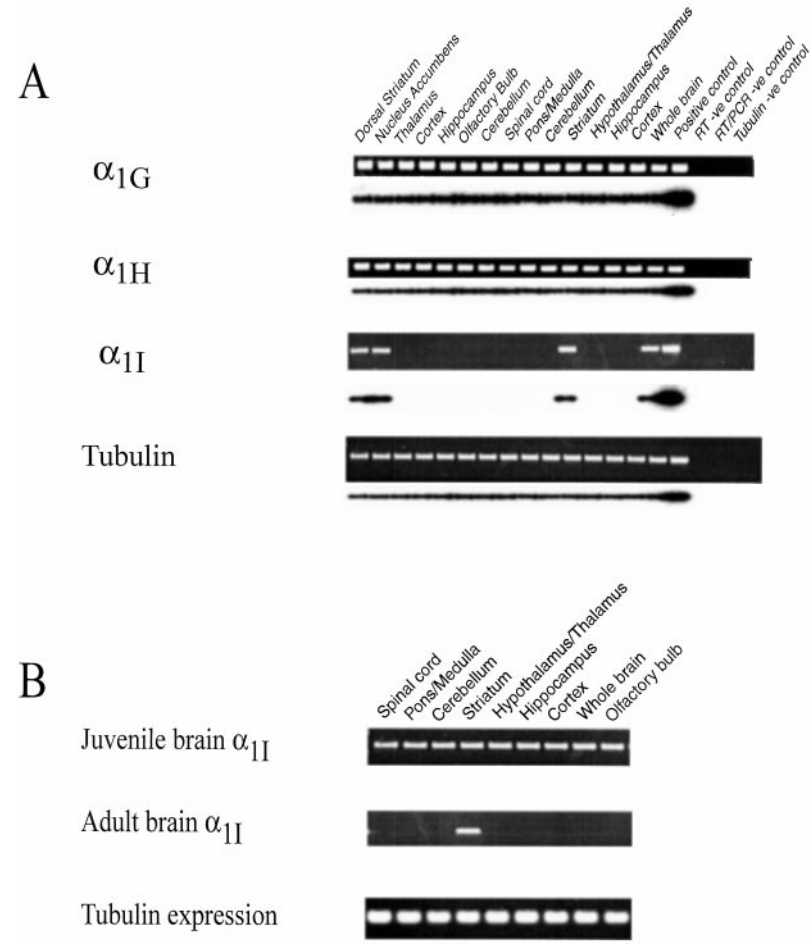

FIG. 4. **RT-PCR to detect α_{1G}, α_{1H}, and α_{1I} T-type calcium channels in rat brain RNA.** *A*, 1 μg of total adult rat RNA was used in the RT-PCR with oligonucleotides specific to α_{1G}, α_{1H}, α_{1I}, and α-tubulin. *B*, RT-PCR to detect α_{1I} and tubulin mRNA in 1 μg of RNA isolated from juvenile rat brain regions. PCR products were electrophoresed through a 1% agarose gel, blotted to nylon membrane, and probed with a [γ-^{32}P]ATP radiolabeled oligonucleotide specific to each channel subtype.

that all four α_{1I} variants are expressed in the rat CNS (data not shown).

Regional expression of the α_{1G}, α_{1H}, and α_{1I} subunits was carried out by Northern blot using the unique domain II-III linkers of each channel as a probe and total RNA isolated from different brain regions of adult rats. The α_{1G} probe (Fig. 3*A*) hybridized to a single band at ~ 10 kb in all brain regions, while the α_{1H} probe hybridized (Fig. 3*B*) to a single band at ~8.5 kb in all brain regions. In contrast, the α_{1I} probe hybridized to an ~11-kb mRNA found only in the adult striatum (Fig. 3*C*). No α_{1I} mRNA signal was detected in total RNA isolated from the different brain regions upon exposure of the autoradiogram for a further 7 days at −80 °C with intensifying screens.

The selective expression of α_{1I} mRNA in the adult striatum is in contrast to the widespread distribution of α_{1I} expression previously reported (23). In an attempt to detect lesser amounts of mRNA than that possible with Northern blots, RT-PCR was performed on the same brain RNA samples. Fig. 4*A* shows that the RT-PCR results confirm the Northern blot results, with α_{1I} mRNA being detected specifically in the adult striatum and α_{1G} and α_{1H} expressed ubiquitously throughout the adult rat brain. Fig. 4*B* shows RT-PCR to compare α_{1I} transcripts using total RNA isolated from 6-week-old and adult rat brain. Within the juvenile rat brain α_{1I} is expressed in all brain regions, while again α_{1I} is selectively expressed in the striatum in adult brain. Taken together, these results suggest the differential expression of α_{1I} calcium channels during CNS development.

Functional Characteristics of α_{1G}, α_{1H}, and α_{1I} Calcium Currents—Transient expression in HEK cells showed that consistent with low voltage-activated channels the mean current-voltage relationships of the α_{1I}, α_{1G}, and α_{1H} channels all activate at negative potentials (Fig. 5*a*). All recordings were carried out using 2 mM calcium as a charge carrier and resulted from the expression of individual α_1 subunits alone. Currents were evoked from a holding potential of −110 mV to voltages from −90 to 0 mV for α_{1H} and α_{1I} and from −80 to 0 mV for α_{1G}. Typically, the threshold for current activation under these ionic conditions was between −80 and −60 mV with peak amplitudes occurring between −45 and −35 mV. Fig. 5, *b–d*, illustrates representative current traces of the three T-type calcium channels obtained during 150-ms test pulses from −90 to 0 mV. All of the channels show substantial inactivation during the test pulse, although α_{1I} shows much slower activation and inactivation kinetics than α_{1G} and α_{1H}. Upon coexpression with the β_{1b} and $\alpha_2\delta$ subunits associated with the HVA calcium channels, we did not observe any functional effects on current-voltage relations, steady-state inactivation, or channel kinetics (data not shown).

Kinetics of Activation and Inactivation—To further examine the voltage dependence of the kinetic parameters, records from each channel subtype were obtained at different potentials, and both the activation time constant (τ_{act}) and the inactivation time constant (τ_{inact}) were measured. To quantify macroscopic activation and inactivation rates, we fitted single-exponential functions to the activating and inactivating segments of individual test currents. Superimposing current traces revealed distinct activation and inactivation kinetics of the three channel types (Fig. 6*a*). The α_{1I} T-type calcium channel activated and inactivated more slowly than the other two channels, while α_{1G} possessed the fastest activation and inactivation kinetics.

Typical of native T-type calcium currents (3), each of the cloned rat brain channels showed marked voltage-dependent

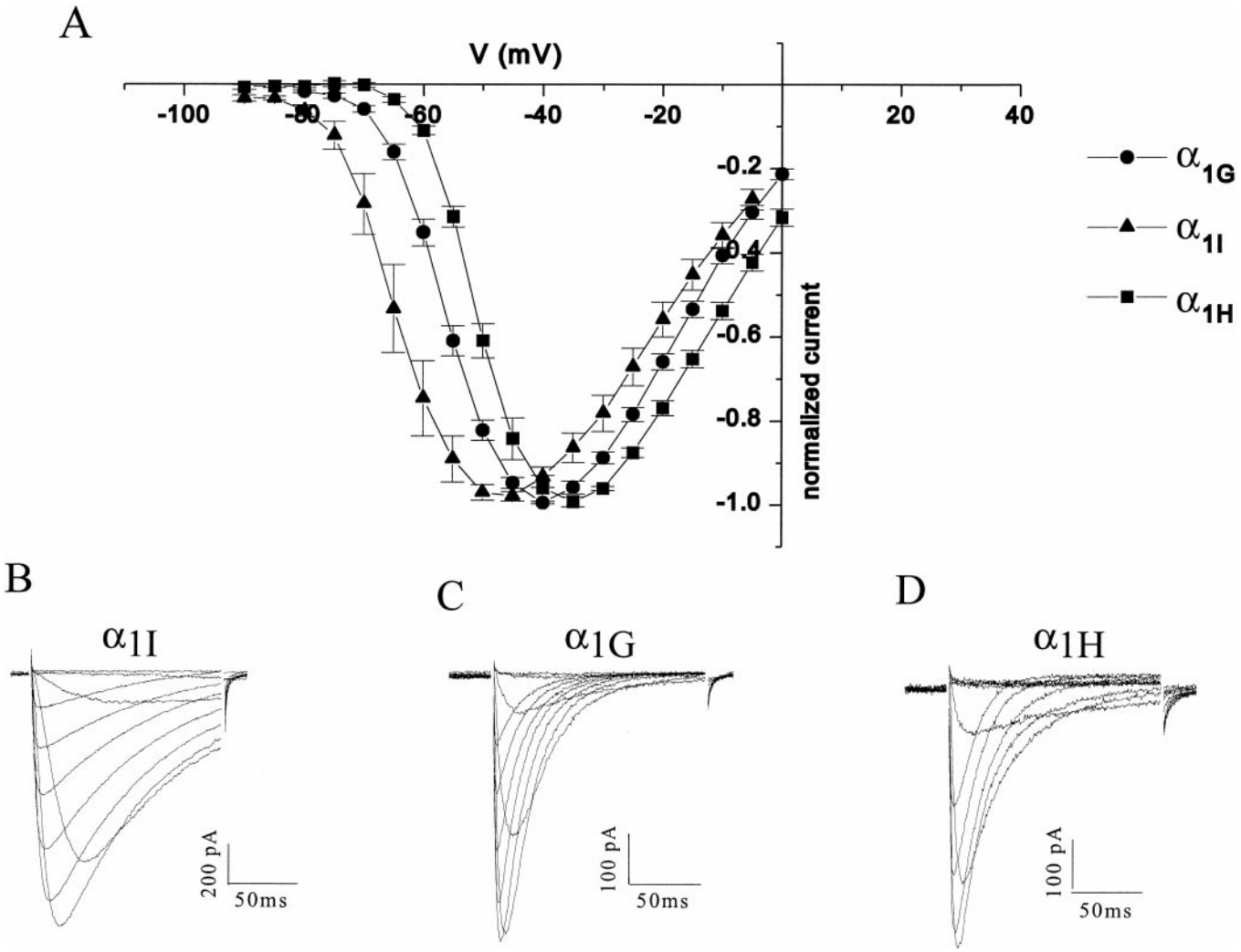

FIG. 5. **Voltage dependence of α_{1I}, α_{1G}, and α_{1H} currents.** *A*, mean current-voltage relationships of Ca^{2+} currents recorded in HEK cells transfected with α_{1I} (*filled triangles*), α_{1G} (*filled circles*), and α_{1H} (*filled squares*). Data were normalized to the peak current observed in each cell and represent the mean ± S.E. from the following number of cells: α_{1I} ($n = 5$), α_{1G} ($n = 13$), α_{1H} ($n = 9$). *B–D*, representative traces of α_{1I} (*B*), α_{1G} (*C*), and α_{1H} (*D*) calcium currents evoked by stepping membrane potential for 150 ms to voltages between −90 and 0 mV in 10 mV increments, from a holding potential of −110 mV. All recordings were done using 2 mM calcium as a charge carrier.

kinetics as both τ_{act} and τ_{inact} decreased markedly at more positive potentials (Fig. 6, *b–g*). The τ_{act} for α_{1G} decayed 76.1% from −45 to −10 mV ($n = 13$), while in the same range of voltage for α_{1H} and α_{1I} the decreases in τ_{act} were 77.6% ($n = 9$) and 52.0% ($n = 4$), respectively. The decrease in τ_{inac} for α_{1G} was 51.7% ($n = 4$) and 31% for α_{1I} ($n = 5$) in the range of −55 to −25 mV. The α_{1H} channel had a larger decrease of 59% from −50 to −25 mV ($n = 9$). Both τ_{act} and τ_{inac} decayed monotonically with voltage toward a voltage-independent minimum. This suggests that voltage-independent transitions must exist in the pathway from the closed to the open state and from the activated to the inactivated states in these calcium channels (35, 36). It is possible that the inactivation process is voltage-independent and kinetically coupled to the activation process as has been suggested by Serrano *et al.* (37).

Voltage Dependence of Activation and Steady-state Inactivation—A more detailed analysis of the voltage-dependent parameters revealed distinct differences between the three rat brain T-type calcium channels. Activation curves for each channel are plotted in Fig. 5*a* and show that α_{1I} activation occurs between −80 and −40 mV, with a $V_{0.5a}$ of −60.7 mV and k_a = 8.39 ($n = 6$); α_{1G} between −70 and −30 mV with $V_{0.5a} = -51.73$ and $k_a = 6.53$ ($n = 5$); and α_{1H} between −55 and −25 mV with $V_{0.5a} = -43.15$ and $k_a = 5.34$ ($n = 9$).

As shown in Fig. 7*b*, inactivation occurs in the range of −105 to −75 mV, −100 to −70 mV, and −80 to −65 mV for α_{1I}, α_{1G}, and α_{1H}, respectively. The $V_{0.5i}$ and k_i values were −93.2 mV and 4.7 ($n = 6$), −85.4 mV and 5.4 ($n = 5$), and −73.9 mV and 2.76 ($n = 4$) for α_{1I}, α_{1G}, and α_{1H}, respectively. The activation and steady-state inactivation curves are similar to those of the native T-type calcium currents present in a variety of excitable and nonexcitable cells (3, 5–20).

To examine window currents, the activation and inactivation curves were plotted for each channel (Fig. 7, *c–e*). The results suggest that although channel open probability is likely to be low, incomplete inactivation and the high driving force for calcium may permit a significant and continuous influx of calcium into the cells within the voltage range of the window current. It is also noticeable that the window currents occur at a negative range of voltages for the three T-type calcium channels close to the value of the resting potential of many cell types.

Deactivation Kinetics—One distinguishing feature of native T-type channels is their slow rate of deactivation after removal of membrane depolarization. The time constant of the decay is ~10 times slower for LVA channels (2–12 ms) (3, 10) than for HVA channels (<300 μs) (38, 39). The rate of deactivation, which reflects the rate of channel closing, was measured as the

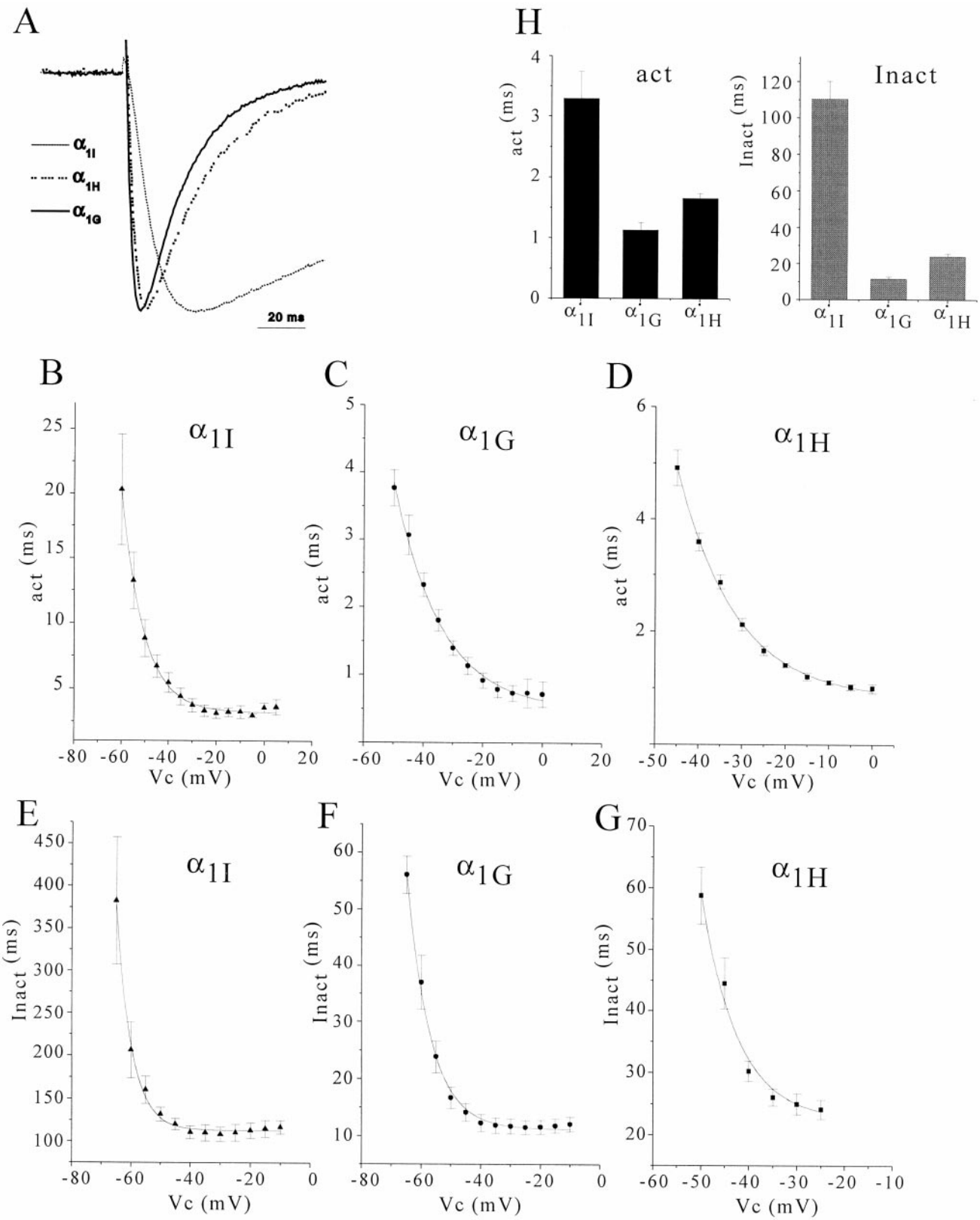

FIG. 6. **Voltage dependence of kinetics parameters of activation and inactivation.** *A*, current traces illustrating a comparison of the temporal course of α_{1I}, α_{1G}, and α_{1H}. Traces were taken at the peak of the IV, normalized and superimposed for comparison. *B–D*, plot of mean values for activation constant (τ_{act}) against command voltage (V_c) for α_{1I} ($n = 4$), α_{1G} ($n = 13$), and α_{1H} ($n = 9$). *Smooth lines* correspond to an exponential fit of the data with an *e*-fold change per 9.34, 15.8, and 13.27 mV for α_{1I}, α_{1G}, and α_{1H}, respectively. *E–G*, plot of mean values for inactivation time constant (τ_{inac} obtained by fitting a single exponential to the decay phase of calcium current) against command voltage for α_{1I} ($n = 5$), α_{1G} ($n = 4$), and α_{1H} ($n = 9$). *Smooth lines* indicate single exponential voltage-dependence of τ_{inac} with *e*-fold change per 5.16, 7.85, and 7.46 mV for α_{1I}, α_{1G}, and α_{1H}, respectively. *Error bars* represent S.E. *H*, plot of mean values of τ_{act} and τ_{inact} at −25 mV.

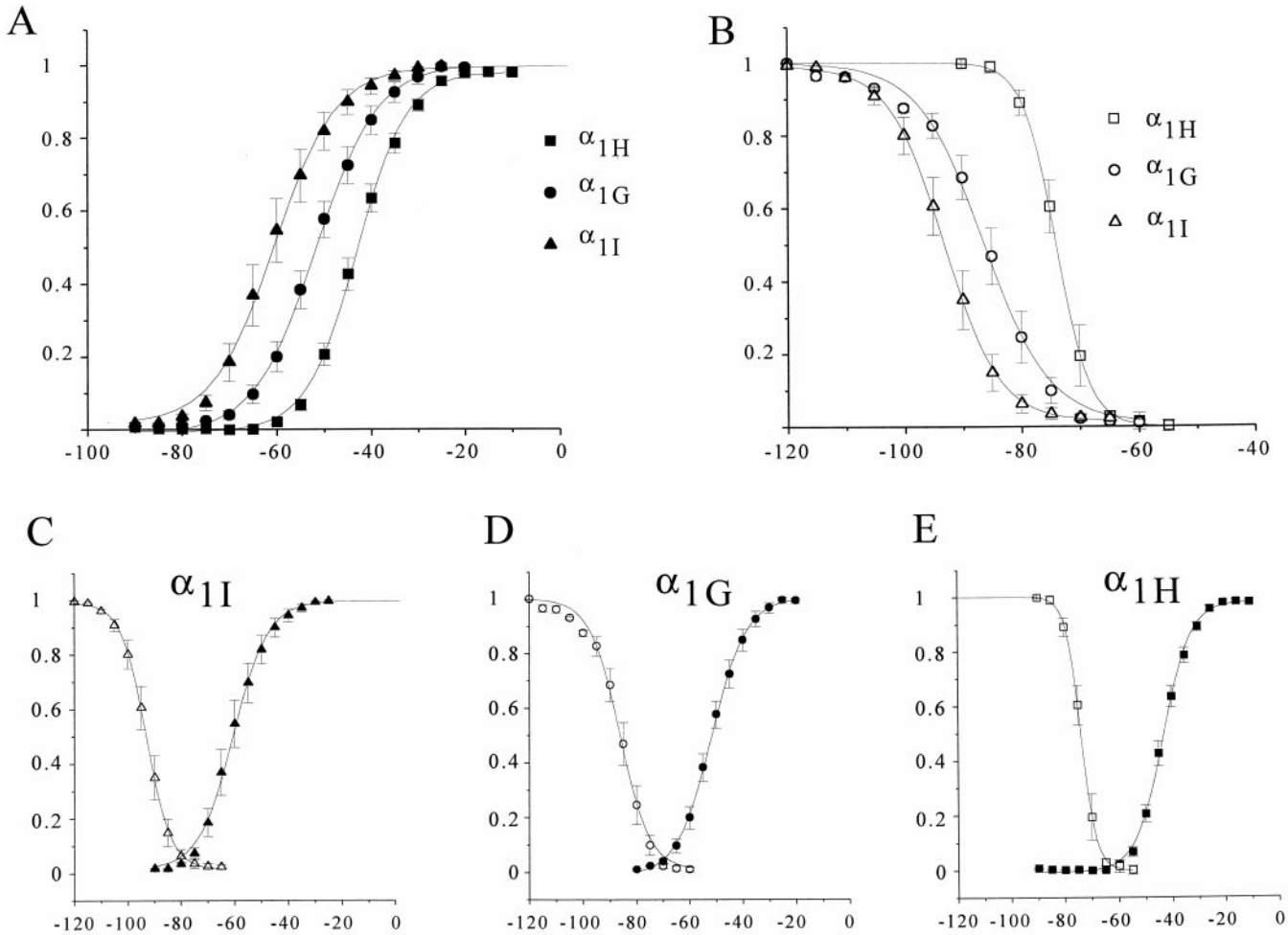

FIG. 7. **Voltage-dependent activation and steady-state inactivation of α_{1I}, α_{1G}, and α_{1H} calcium currents.** *A*, activation curves. The current amplitude was converted to conductance by assuming a calcium reversal potential extrapolated from the linear, positive slope region of the *I*-V curve. The conductance at each potential was normalized to the maximum conductance and was averaged for each step potential. The *symbols* represent pooled data from α_{1I} (*filled triangles*, $n = 5$), α_{1G} (*filled circles*, $n = 4$), and α_{1H} (*filled squares*, $n = 9$). *Solid lines* represent the fitting with Boltzman equations with half-activation voltages ($V_{0.5a}$) of −60.7, −51.73, and −43.15 mV and slope factors (k_a) of 8.39, 6.53, and 5.34 for α_{1I}, α_{1G}, and α_{1H}, respectively. *B*, steady-state inactivation curves. The membrane potential was stepped to −30 mV from holding potentials ranging from −120 to −50 mV. The normalized peak amplitude of the currents elicited by the test pulse to −30 mV was plotted as a function of the holding potential. These data were fitted with a Boltzman equation (*smooth curves*). Half-inactivation voltage ($V_{0.5i}$) and slope factor (k_i) were −93.2 mV and 4.7 ($n = 6$), −85.4 mV and 5.4 ($n = 5$), and −73.9 mV and 2.76 ($n = 4$) for α_{1I} (*open triangles*), α_{1G} (*open circles*), and α_{1H} (*open squares*), respectively. *c–e*, activation and inactivation curves were plotted in the same graphic and expanded to show window currents for each channel: α_{1I} (*C*), α_{1G} (*D*), and α_{1H} (*E*).

rate of decay of the tail currents at different repolarizing potentials. Tail currents of α_{1I}, α_{1G}, and α_{1H} were fitted with single exponentials, whose time constants of decay (τ_{deac}) decreased at more negative repolarization potentials (Fig. 8*a*). At −120 mV, the values for τ_{deac} were 1.63 ± 0.1 ($n = 3$), 1.15 ± 0.073 ($n = 6$), and 0.61 ± 0.82 ($n = 4$) for α_{1G}, α_{1I}, and α_{1H}, respectively. Fig. 8, *b–d*, shows the tail currents obtained during different repolarizing pulses from −120 to −40 mV applied after a test pulse of −40 mV for α_{1G} and α_{1I} and −30 mV for α_{1H}. The kinetics of the tail currents for all three T-type channels were faster at more negative repolarizing potentials, indicating a strong voltage dependence of the deactivation process. The slow rate of deactivation would allow a significant calcium influx after short action potentials (40), enabling neurons to control their excitability by regulating the activation of calcium-dependent potassium channels responsible for the after potentials hyperpolarizing.

Barium Versus Calcium Permeability—Typically, native T-type calcium channels have been characterized by their distinct permeability to divalent ions. In most instances, T-type channels are either equally permeable or more permeable to calcium than barium, usually indicated by a smaller whole-cell current when barium is used a charge carrier (8, 41–43). In HEK cells transfected with α_{1G} (Fig. 9), substitution of 2 mM calcium with 2 mM barium resulted in a significant decrease in the current amplitude and a small shift of the *I*-V curve in the hyperpolarized direction ($V_{0.5} = -45$ mV in 2 mM Ba, $V_{0.5} = -52.4$ in 2 mM calcium, $n = 3$). Cells transfected with α_{1I} showed equivalent amplitude currents when 2 mM calcium was replaced by 2 mM barium, without a significant shift in the *I*-V curve ($n = 8$). Most interestingly, rat α_{1H} had significantly larger currents in 2 mM barium than in 2 mM calcium ($n = 7$). At all potentials explored, there were no major changes in the kinetics of α_{1G}, α_{1H}, and α_{1I} currents using the different charge carriers (data not shown).

DISCUSSION

This study is the first both to describe the molecular cloning and functional expression of three T-type calcium channel α_1 subunits (α_{1G}, α_{1H} and α_{1I}) from the same species and tissue and to compare their biophysical properties in 2 mM calcium saline. We find significant molecular and functional differences

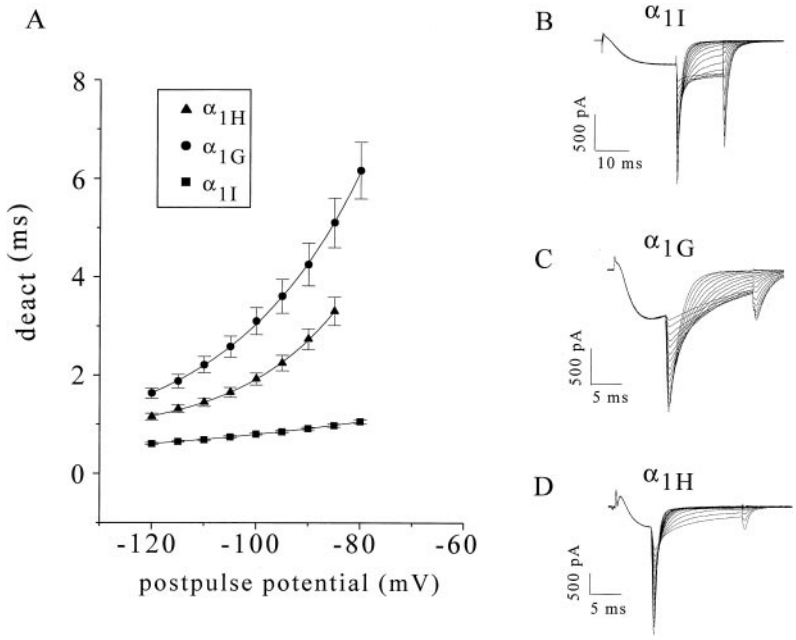

FIG. 8. **Voltage dependence of deactivation kinetics.** *A*, plot of mean deactivation time constants (τ_{deac}) against repolarization potentials. Data represent mean and S.E. for the following number of cells: α_{1I} ($n = 6$), α_{1G} ($n = 3$), and α_{1H} ($n = 4$). Deactivation time constants were determined by fitting tail currents (*B–D*) with a single exponential. *B–D*, representative calcium current tail traces of α_{1I} (*B*), α_{1G} (*C*), and α_{1H} (*D*). Currents were evoked using the following voltage protocols: a 9-ms step to −40 mV for α_{1G}, a 20-ms step to −50 mV for α_{1I}, and a 6-ms step to −30 mV for α_{1H} followed by repolarization to potentials from −120 to −40 mV.

between the channel types that may help both in understanding the diversity of native T-type channels and in elucidating their physiological roles. The major novel insights include 1) that at least four alternatively spliced variants of the α_{1I} T-type calcium channel are expressed in the CNS, 2) that, compared with the α_{1G} and α_{1H} T-type channels, α_{1I} exhibits a distinct developmental and spatial expression profile, 3) that in identical external 2 mM calcium saline the α_{1G} and α_{1I} T-type channels exhibit voltage-dependent properties that are significantly different from those previously reported, and 4) that modeling of the α_{1G}, α_{1H}, and α_{1I} channels in thalamic relay neurons indicates that the three T-type channels probably contribute to distinct oscillatory and bursting behaviors.

Northern blot and RT-PCR experiments examining juvenile brain regions showed that the $\alpha_{1G,}$ α_{1H}, and α_{1I} T-type calcium channels were expressed ubiquitously in the spinal cord, cerebellum, pons/medulla, striatum, hypothalamus/thalamus, hippocampus, cortex, and olfactory bulb (Figs. 3 and 4*B*). It has been suggested that T-type calcium channels have a role in tissue development, and reports for vascular smooth muscle suggest that T-type channels are expressed only during the G_1-S phase of the cell cycle (for a review, see Ref. 3). The widespread expression of the three different T-type channels in the juvenile rat brain suggests possible roles in cell division, growth, and proliferation of the nervous system.

In the adult nervous system, while α_{1G} and α_{1H} were expressed in all brain regions examined, α_{1I} transcripts were selectively expressed in the striatum. Our results for α_{1G} and α_{1H} are essentially in agreement with those reported by Talley *et al.* (23), who showed high to moderate α_{1G} and α_{1H} expression in the olfactory bulb, hippocampus, striatum, cortex, thalamus and hypothalamus, and, to a lesser extent, in the sensory ganglia. However, in contrast to our studies, Talley *et al*. (23) reported the widespread expression of the α_{1I} T-type channel in many adult rat brain regions. Furthermore, while Perez-Reyes *et al.* (21) reported that α_{1G} hybridizes to two mRNAs of ~8.5 and 9.7 kb in rat brain, we find that α_{1G} only hybridizes to a single ~10-kb mRNA. Interestingly, the 8.5-kb α_{1G} mRNA reported previously (21) is similar in size to that for α_{1H} and suggests the possibility of probe cross-reaction. Previous electrophysiological studies have shown that a small percentage of adult rat neostriatal neurons have measurable LVA calcium currents (44, 45). It is likely that α_{1I} constitutes at least some of the native LVA current in these striatal neurons and that this channel may be involved in the burst firing typical of type I globus pallidus neurons (Ref. 46; also see Fig. 10).

In comparing the primary structure of the rat brain α_{1G}, α_{1H}, and α_{1I} T-type calcium channels, a prominent difference is the shorter length of the α_{1I} calcium channel. As shown in Fig. 1, the shorter α_{1I} predicted protein is mainly the result of shorter domain I-II linker and carboxyl tail regions. When aligned with the domain I-II linkers of α_{1G} and α_{1H}, the shorter length is the result of α_{1I} possessing several large gaps, most noticeably a gap that omits a histidine repeat found in the α_{1G} and α_{1H}. Another feature of the α_{1I} subunit is the short 77-amino acid carboxyl tail, which is due to a stop codon (TAA) at positions 5458–5460 of the α_{1I} cDNA sequence and which is likely to be the result of alternative splicing (47). The sequence of the rat α_{1I} carboxyl tail reported here is similar to that reported by Lee *et al.* (24) and distinct from the human α_{1I} subunit reported by Monteil *et al.* (48).

We find that at least four α_{1I} T-type variants are expressed in the rat CNS. Transient expression of the $\alpha_{1I\text{-}c}$ and $\alpha_{1I\text{-}d}$ variants in HEK cells shows that they result in functional T-type channels (data not shown), although a detailed analysis of their biophysical properties remains to be undertaken. Taken together, the data suggest that multiple variants of T-type channels are expressed in the CNS. Since single aa substitutions can have dramatic effects on channel properties, it is likely that sequence differences between α_{1G}, α_{1H}, and α_{1I} channels themselves, as well as between isoforms resulting from alternative splicing, probably account for many of the biophysical differences reported for native T-type calcium channels.

Expression of α_{1G}, α_{1H}, and α_{1I} subunits in HEK tsa201 cells produced calcium currents with many characteristics of native T-type channels, although significant differences exist between the three subtypes. For example, α_{1I} channels activate and inactivate at the most negative potentials, while the α_{1H} subtype displays the most positive activation and inactivation voltage range. These results differ from those reported by Klockner *et al.* (49), who showed similar inactivation values for α_{1G}, α_{1H}, and α_{1I} channels. The discrepancy between their and our findings may be explained by the use of different expression systems (transient transfection *versus* stable cell lines), different solution composition, or primary sequence differences aris-

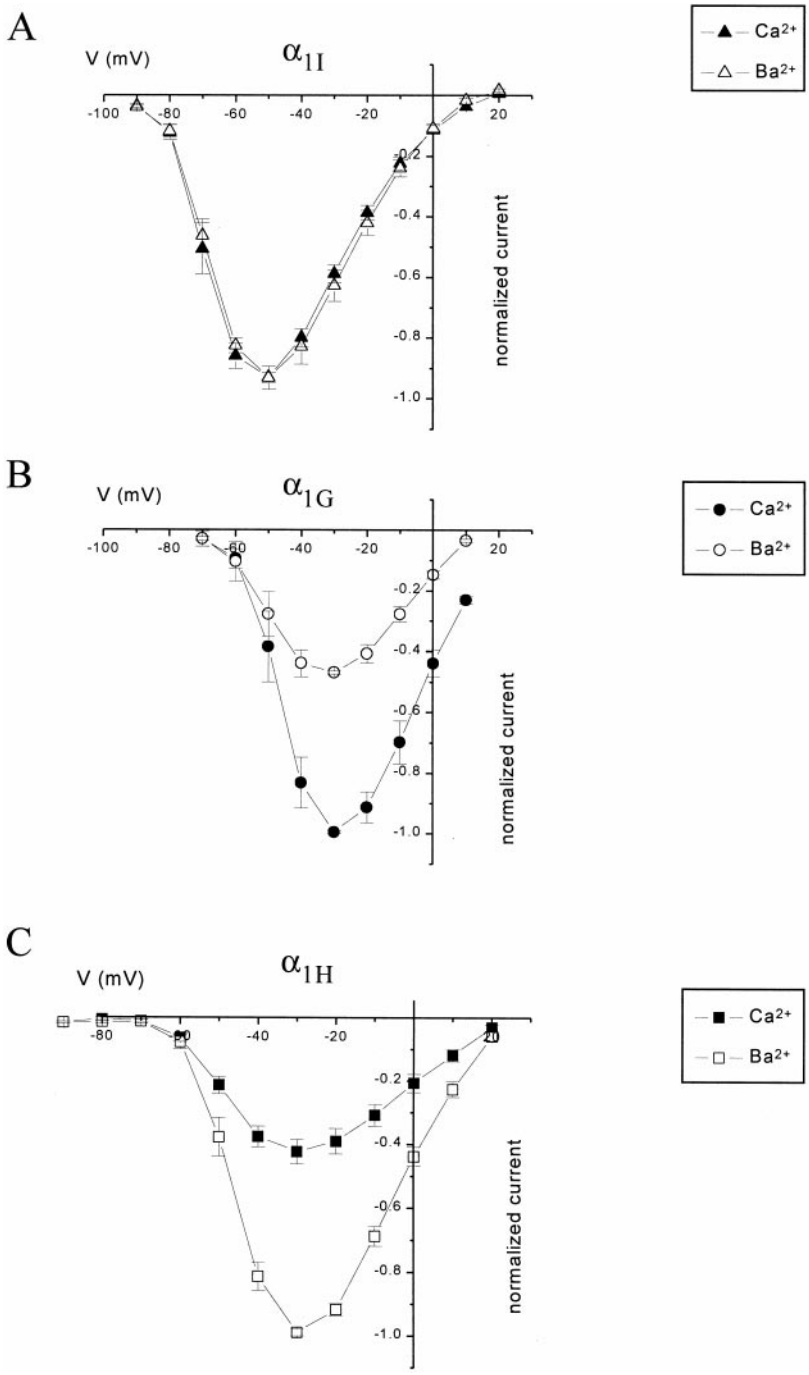

FIG. 9. **barium *versus* calcium permeability.** Shown are mean *I*-V curves obtained in 2 mM barium (*open symbols*) and in 2 mM calcium (*filled symbols*) for α_{1I} (*triangles*, $n = 8$) (*A*), α_{1G} (*circles*, $n = 3$) (*B*), and α_{1H} (*squares*, $n = 7$) (*C*).

ing from different species (human α_{1H} was used in the Klockner *et al.* study and rat α_{1H} in the present study). Our results also differ from those of Monteil *et al.* (48), who showed that the human α_{1I} activated and inactivated at more positive potentials compared with the human α_{1G}.

In addition to voltage-dependent differences, channel kinetics were also distinct for each of the three rat brain T-type calcium channels; α_{1G} activated and inactivated with the fastest kinetics, while α_{1I} exhibited the slowest kinetics. Most native T-type calcium channels exhibit inactivation time courses with τ_h values in the range of the α_{1G} and α_{1H} inactivation time constants. However, some native T-type channels with kinetics similar to α_{1I} have been described in thalamus and hippocampus (3). It has been suggested that α_{1I} might correspond to the slow T-type channel present in juvenile thalamic reticular neurons (24, 57), although our results indicate significant differences between α_{1I} and the native thalamic slow T-type channel. For example, α_{1I} exhibits slower inactivation kinetics ($\tau_h = 112.8$ ms at -20 mV compared with ~80 ms for the native T-type slow current), more negative activation and inactivation characteristics, and importantly, also possesses a different divalent ion permeability profile than the slow T-type current in thalamic reticular neurons (Ref. 24; see Fig. 9).

Human neuronal α_{1G} and α_{1I} T-type channels have recently been characterized (48, 50). Comparison of the human and rat α_{1G} properties shows that they share some similarities, including activation threshold and inactivation and deactivation kinetics, although they significantly differ in their steady-state inactivation profiles ($V_{0.5} = -86$ mV for rat *versus* -75 mV for human). Comparison of the rat and human α_{1I} channels shows that the human α_{1I} activates and inactivates at more positive

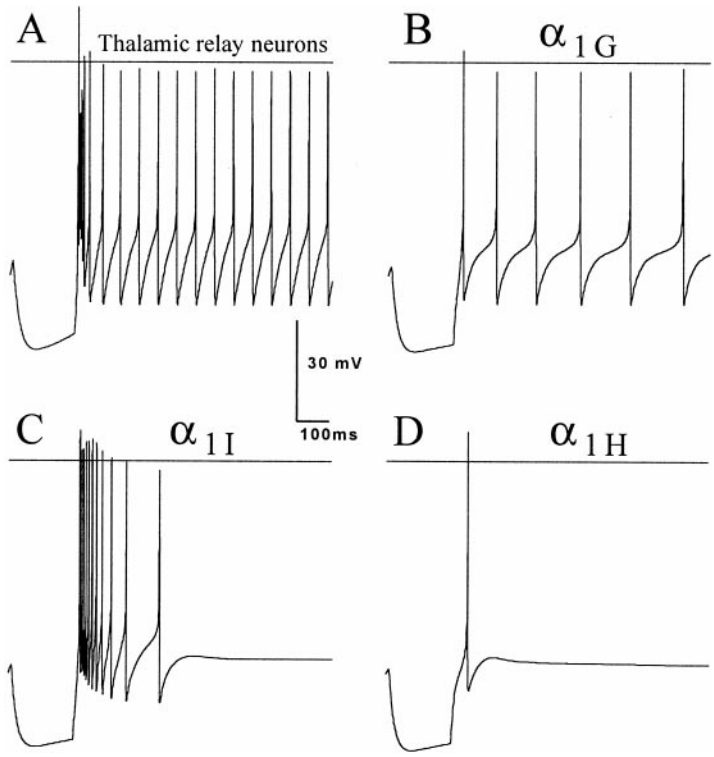

FIG. 10. **Simulated current clamp recordings of thalamic neurons containing α_{1G}, α_{1H}, and α_{1I} T-type channels.** *A*, rebound spikes generated by stimulation with 500 pA of hyperpolarizing current for 200 ms in juvenile thalamic relay neurons (29, 30). *B*, substitution of α_{1G} for the native T-type currents in the model cell generates oscillatory spiking behavior. *C*, in contrast to α_{1G}, α_{1I} substitution elicits rebound burst spiking in the simulated thalamic neuron. *D*, the replacement of native T-type current parameters with those of α_{1H} caused only a single rebound spike in response to hyperpolarization.

potentials ($V_{0.5}$ activation = −40.6 mV for human α_{1I} *versus* −60.7 mV for rat α_{1I}). Additionally, the steady-state inactivation profile of the rat α_{1I} is significantly more negative ($V_{0.5}$ = −93.2 mV) compared with that for the human α_{1I} ($V_{0.5}$ = −68.9).

T-type channels typically deactivate ~10 times slower than HVA calcium channels, including R-type channels (51). In agreement, the three rat brain T-type channels were found to deactivate slowly with τ_{deac} values of 1.63, 1.1, and 0.61 ms for α_{1G}, α_{1I}, and α_{1H}, respectively. This observation is in agreement with the results reported for α_{1G} and α_{1I} by Klockner *et al.* (49). However, in contrast to the human α_{1H} T-type channel, we found that the rat α_{1H} deactivated faster than the other two rat brain T-type channels. Moreover, we observed only a fast component of the tail current and not the slow component reported by Williams *et al.* (25) for α_{1H} from the human medullary thyroid carcinoma cell line.

All three rat brain T-type channels display a steady-state inward window current over a negative range of potentials that is close to the resting potentials of many cell types. A continuous influx of calcium at resting potentials through T-type channels may play a significant role in cellular physiology and has been implicated in mediating cell growth and proliferation in response to growth factors in cardiac cells (52), in the secretion of aldosterone in adrenal granulosa cells (18), and in maturation and differentiation of spermatogenic cells (53). Additionally, an increase in the window current of T-type calcium channels has been implicated in the pathophysiology of genetic cardiomyopathy in hamsters (54), in cytokine-induced pancreatic beta cell death (55), and in motor neuronal toxicity in spinobulbar muscular atrophy (56).

Generally T-type calcium channels display divalent ion permeation characteristics such that peak currents are either similar or smaller upon replacement of calcium with barium (3, 8, 41–43). In agreement, in this study we showed that both α_{1G} and α_{1I} peak whole-cell currents were smaller or similar when barium replaced calcium as the charge carrier. In contrast, α_{1H} displayed larger whole-cell currents in barium than in calcium. Our findings for α_{1H} differ from those of Williams *et al.* (25), who showed that human α_{1H} from a medullary thyroid carcinoma cell line possesses larger currents when calcium is used as the charge carrier. Examination of the residues implicated in selectivity (the aspartates and glutamates in the P-loops) did not suggest any obvious differences in human and rat α_{1H} subunits that could explain their distinct permeabilities. The only noticeable change between the human α_{1H} and rat α_{1H} P-loops is a serine to threonine substitution at the beginning of the P-loop of domain IV.

Although similar efficiency of calcium and barium as current carriers is generally characteristic of the T-type calcium channels, there are examples of T-type currents in native cells that are more permeable to barium than to calcium. One example is the T-type current present in rat thalamic reticular neurons (57). It has been recently reported by Serrano *et al.* (58) that conductance differences between calcium and barium through α_{1G} channels are due to distinct effects of magnesium on calcium and barium currents. These authors showed a voltage-dependent block with 1 mM magnesium preferentially affected inward current carried by barium. However, in the present study α_{1H}, barium and calcium currents were recorded both in the presence and absence of external magnesium, and whole-cell peak barium currents were still larger than calcium currents (data not shown).

In thalamic neurons, the generation of bursting activity appears to be a major function of the T-type channels, although this type of electrical behavior differs greatly between neurons in different thalamic nuclei (3). For example, thalamic reticular neurons display longer lasting bursting behavior as compared with thalamic relay neurons (29, 57). To correlate the properties of the three rat brain T-type calcium channels described in this study with native thalamic T-type currents, we substituted the electrophysiological properties of α_{1G}, α_{1H}, and α_{1I} for the properties of the native T-type current in a simulated model of a juvenile thalamic relay neuron (29, 30).

As shown in Fig. 10, the model thalamic relay neurons have a distinct rebound spiking profile, which consists of a high frequency burst followed by lower frequency oscillatory spikes. Substitution of α_{1G} for the native channel in the model causes

the oscillatory firing pattern to decrease in frequency, and the high frequency bursts are eliminated. An electrophysiological comparison of α_{1G} with the native T-type channel in thalamic relay neurons (29) indicates many similarities but enough differences to alter the role in modifying electrical behavior. Interestingly, α_{1I}-substituted model neurons showed distinct high frequency burst firing typical of many types of thalamic neurons including juvenile thalamic reticular neurons (3). Also of interest, the rat α_{1H} T-type channel only produced a single rebound spike in this model thalamic cell. Taken together, these studies suggest that the three classes of rat brain T-type channels are likely to make distinct contributions to cellular electrical properties and intracellular calcium levels and that they play unique roles in neuronal physiology and development.

REFERENCES

1. Catterall, W. A. (1995) *Annu. Rev. Biochem.* **64,** 493–531
2. Stea, A., Soong, T. W., and Snutch T. P. (1995) *Handbook of Receptors and Channels: Ligand- and Voltage-gated Ion Channels* (North, R. A., ed) pp. 113–151, CRC Press, Inc., Boca Raton, FL
3. Huguenard, J. R. (1996) *Annu. Rev. Physiol.* **58,** 329–348
4. Llinas, R., and Yarom, Y. (1981) *J. Physiol.* (*Lond.*) **315,** 549–567
5. Carbone, E., and Lux H. D. (1984) *Biophys. J.* **46,** 413–418
6. Carbone, E., and Lux H. D. (1984) *Nature* **310,** 501–502
7. Bossu, J.-L., Feltz, A., and Thomann, J. M. (1985) *Pfluegers Arch.* **403,** 360–368
8. Fedulova, S. A., Kostyuk, P. G., and Veselovsky, N. S. (1985) *J. Physiol.* (*Lond.*) **359,** 431–446
9. Nowycky, M. C., Fox, A. P., and Tsien, R. W. (1985) *Nature* **316,** 440–443
10. Matteson, D. R, and Armstrong, C. M. (1986) *J. Gen. Physiol.* **8,** 161–182
11. Mason, W. T., and Sikdar, S. K. (1989) *J. Physiol.* (*Lond.*) **415,** 367–391
12. Bean, B. P. (1985) *J. Gen. Physiol.* **86,** 1–30
13. Nilius, B., Hess, P., Lansman, J. B., and Tsien, R. W. (1985) *Nature* **316,** 443–446
14. Hagiwara, N., Irisawa, H., and Kameyama, M. (1988) *J. Physiol.* (*Lond.*) **395,** 233–253
15. Nuss, H. B., and Houser, S. R. (1993) *Circ. Res.* **73,** 777–782
16. Zhou, Z., and Lipsius. (1994) *J. Mol. Cell. Cardiol.* **26,** 1211–1219
17. McCleskey, E. W., and Schroeder, J. E. (1991) *Curr. Top. Membr.* **39,** 295–326
18. Cohen, C. J., McCarthy, R. T., Barrett, P. Q., and Rasmussen, H. (1988) *Proc. Natl. Acad. Sci. U. S. A.* **85,** 2412–2416
19. Enyeart, J. J., Mlinar, B., and Enyeart, J. A. (1993) *Mol. Endocrinol.* **7,** 1031–1040
20. Akaike, N., Kostyuk, P. G., and Osipchuk, Y. V. (1989) *J. Physiol.* (*Lond.*) **412,** 181–195
21. Perez-Reyes, E., Cribbs, L. L., Daud, A., Lacerda, A. E., Barclay, J., Williamson, M. P., Fox, M., Rees, M., and Lee, J. H. (1998) *Nature* **391,** 896–900
22. Cribbs, L. L., Lee, J. H., Yang, J., Satin, J., Zhang, Y., Daud, A., Barclay, J., Williamson, M. P., Fox, M., Rees M., and Perez-Reyes, E. (1998) *Circ. Res.* **83,** 103–109
23. Talley, E. M., Cribbs, L. L., Lee, J. H., Daud, A., Perez-Reyes, E., and Bayliss, D. A. (1999) *J. Neurosci.* **19,** 1895–1911
24. Lee, J. H., Daud, A. N, Cribbs, L. L, Lacerda, A. E, Pereverzev, A., Klockner, U., Schneider, T., and Perez-Reyes, E. (1999) *J. Neurosci.* **19,** 1912–1921
25. Williams, M. E., Washburn, M. S., Hans, M., Urrutia, A., Brust, P. F., Prodanovich, P, Harpold, M. M., and Stauderman, K. A. (1999) *J. Neurochem.* **72,** 791–798
26. Snutch, T. P., Leonard, J. P., Gilbert, M. M., Lester, H. A., and Davidson, N. (1990) *Proc. Natl. Acad. Sci. U. S. A.* **87,** 3391–3395
27. Sutton, K. G., McRory, J. E., Guthrie, H., Murphy, T. H., and Snutch, T. P. (1999) *Nature* **401,** 800–804
28. Hamill O. P., Marty, A., Neher, E., Sakmann, B., and Sigworth, F. J. (1981) *Pfluegers Arch.* **391,** 85–100
29. Huguenard, J. R., and McCormick, D. A. (1992) *J. Neurophysiol.* **68,** 1373–1383
30. McCormick, D. A., and Huguenard, J. R. (1992) *J. Neurophysiol.* **68,** 1384–1400
31. Pragnell, M., De Waard, M., Mori, Y., Tanabe, T., Snutch, T. P., and Campbell, K. P. (1994) *Nature* **368,** 67–70
32. Babitch, J. (1990) *Nature* **346,** 321–322
33. Lee, A., Wong, S. T., Gallagher, D., Li, B., Storm, D. R., Scheuer, T., and Catterall, W. A. (1999) *Nature* **399,** 155–159
34. Peterson, B. T., DeMaria, C. D., Adelman, J. P., and Yue, D. T. (1999) *Neuron* **22,** 549–558
35. Chen, C., and Hess, P. (1990) *J. Gen. Physiol.* **96,** 603–630
36. Mlinar, B., Biagi, B. A., and Enyeart, J. J. (1993) *J. Gen Physiol.* **102,** 217–237
37. Serrano, J. R., Perez-Reyes, E., and Jones, S. W. (1999) *J. Gen Physiol.* **114,** 185–201
38. Swandulla, D., and Armstrong, C. M. (1988) *J. Gen. Physiol.* **92,** 197–218
39. Williams, M. E., Marubio, L. M. Deal, C. R., Hans, M., Brust, P. F., Philipson, L. H., Miller, R. J., Johnson, E. C., Harpold, M. M., and Ellis, S. B. (1994) *J. Biol. Chem.* **269,** 22347–22357
40. McCobb, D. P., and Beam, K. G. (1991) *Neuron* **7,** 119–127
41. Carbone, E., and Lux, H. D. (1987) *J. Physiol.* (*Lond.*) **386,** 547–570
42. Carbone, E., and Lux, H. D. (1987) *J. Physiol.* (*Lond.*) **386,** 571–601
43. Fox, A. P., Nowycky, M. C., and Tsien, R. W. (1987) *J. Physiol.* (*Lond.*) **394,** 149–172
44. Hoehn, K., Watson, T. W., and MacVicar, B. A. (1993) *J. Neurosci.* **13,** 1244–1257
45. Bargas, J., Howe, A., Eberwine, J., Cao, Y., and Surmeier, D. J. (1994) *J. Neurosci.* **14,** 6667–6686
46. Nambu, A., and Llinas, R. (1994) *J. Neurophysiol.* **72,** 1127–1139
47. Mittman, S., Guo, J., Emerick, M. C., and Agnew, W. S. (1999) *Neurosci. Lett.* **16,** 121–124
48. Monteil, A., Chemin, J., Leuranguer, V., Altier, C., Mennessier, G., Bourinet, E., Lory, P., and Nargeot, J. (2000) *J. Biol. Chem.* **275,** 16530–16535
49. Klockner, U., Lee, J. H., Cribbs, L. L, Daud, A., Hescheler, J., Pereverzev, A., Perez-Reyes, E., and Schneider, T. (1999) *Eur. J. Neurosci.* **11,** 4171–4178
50. Monteil, A., Chemin, J., Bourinet, E., Mennessier, G., Lory, P., and Nargeot, J. (2000) *J. Biol. Chem.* **275,** 6090–6100
51. Randall, A. D., and Tsien, R. W. (1997) *Neuropharmacology* **36,** 879–893
52. Xu, X., and Best, P. M. (1991) *Proc. Natl. Acad. Sci. U. S. A.* **87,** 4655–4659
53. Santi, C. M., Darszon, A., and Hernández-Cruz, A. (1996) *Am. J. Physiol.* **27,** C1583–C1593
54. Bkaily, G., Sculptoreanu, A., Jacques, D., and Jasmin, G. (1997) *Mol. Cell. Biochem.* **176,** 199–204
55. Wang, L., Bhattacharjee, A., Zuo, Z., Hu, F. Q., Honkanen, R. E., Berggren, P. O., and Li, M. (1999) *Endocrinology* **140,** 1200–1204
56. Sculptoreanu, A., Abramovici, H., Abdullah, A. R., Bibikova, A., Panet-Raymond, V., Frankel, D., Schipper, H. M., Pinsky, L., and Trifiro, M. A. (2000) *Mol. Cell. Biochem.* **203,** 23–31
57. Huguenard, J. R., and Prince, D. A. (1992) *J. Neurosci.* **12,** 3804–3838
58. Serrano, J. R., Perez-Reyes, E., and Jones, S. W. (2000) *Biophys. J.* **78,** 445A